Journal of Physics and Chemistry of Solids 144 (2020) 109518

Contents lists available at ScienceDirect

Journal of Physics and Chemistry of Solids

journal homepage: http://www.elsevier.com/locate/jpcs

Organic-inorganic hybrid halide perovskites impregnated with Group 1 and 15 elements for solar cell application

Pritam Dey [a,1], Harish Singh [a,1], Rahul K. Gupta [b], Debabrata Goswami [b], Tanmoy Maiti [a,*]

[a] Plasmonics and Perovskites Laboratory, Department of Materials Science and Engineering, IIT Kanpur, U.P., 208016, India
[b] Department of Chemistry, IIT Kanpur, U.P., 208016, India

ARTICLE INFO

Keywords:
Halide perovskite
Bismuth
Fluorescence decay kinetics
Stability

ABSTRACT

In this report, we explored the substitution of triple cations at B-site of ABX_3 perovskite architecture in inorganic-organic hybrid perovskite materials in order to improve its stability over moisture and heat, which is considered as the paramount obstacles for commercialization of perovskite solar cell. In the current investigation we synthesized two novel perovskite materials, Methylammonium potassium bismuth lead iodide [$CH_3NH_3K_{0.25}Bi_{0.25}Pb_{0.5}I_3$] (MKBPI) and Methylammonium sodium bismuth lead iodide [$CH_3NH_3Na_{0.25}Bi_{0.25}Pb_{0.5}I_3$] (MNBPI). XRD studies confirmed hexagonal crystal structure with $P6_3/mmc$ space group for both the perovskites. Antisolvent treatment improved the surface coverage and morphology of the thin films, observed in FESEM. UV–Vis spectra demonstrated high absorption coefficient. Band gap was estimated as 2.09 eV for MKBPI. Fluorescence decay kinetics study revealed charge carrier lifetime on the order of nano second. DSC and TGA measurements confirmed thermal stability of these perovskites up to 280 °C. Further, we carried out detailed degradation study using XRD and UV–Vis spectroscopy of these perovskite thin films kept at ambient atmosphere for two weeks. Remarkably thin films of these perovskites exhibited good absorption even after 14 days.

1. Introduction

Remarkable increase in power conversion efficiency (PCE) of organic-inorganic hybrid halide based perovskite solar cells (PSC) in the last few years made perovskite materials a primary focus in the field of photovoltaic research [1]. Although the first report on halide based hybrid perovskite compound was made by Dieter Weber in 1978 [2,3], its application to photovoltaics did not uncover until 2009 when Kojima et al. reported first organometallic halide perovskite solar cells, where methylammonium lead halide, $MAPbX_3$ (X = I, Br) solutions were loaded on the top of titanium dioxide mesoporous layer by spin cast [4]. Recently, the energy conversion efficiency surpassed 24% barrier [5]. It was believed that its strong optical absorption owing to s-p anti-bonding coupling, high charge carrier mobility, large carrier diffusion length (>1 μm) and high structural tolerance were the potential reasons for high PCE [6,7]. Furthermore, comparatively good crystallization and easy film formation ability from low temperature solution processing made them highly competitive and promising low cost photovoltaic materials [8]. However, lead based PSCs suffered from environmentally hazardous constituent lead and poor stability over moisture and heat [9–13]. These issues prevented the commercialization of lead based PSCs. Recently, two-dimensional Ruddlesden–Popper (2DRP) lead based perovskites reported to be promising candidate for solar cell applications due to their long-term moisture resistance, and thermal stability [14–16]. To avoid the toxicity of lead-based perovskites, some research works were also initiated towards the development of lead-free PSCs [17,18].

Tin was the first element that was investigated as a potential replacement of lead in the pursuit of lead-free perovskite solar cell [19–23]. However, the fast oxidation of divalent tin cation to its most stable oxidation state of Sn^{4+} reduces the stability of these tin based perovskite structures in air. Bi (6p-block) has outer lone pair $6s^2$ electrons similar to lead (Pb), which plays a significant role to have high Born effective charges. It enhances the screening to charged defects within the material [24]. Reasonable band gap with high relativistic effect makes bismuth halide perovskites a promising alternative [25–27]. In the last couple of years, few reports were made on methylammonium bismuth iodide (MBI) and its derivatives for solar cell

* Corresponding author.
E-mail address: tmaiti@iitk.ac.in (T. Maiti).
[1] Authors with equal contribution.

https://doi.org/10.1016/j.jpcs.2020.109518
Received 14 December 2019; Received in revised form 15 March 2020; Accepted 18 April 2020
Available online 23 April 2020

applications [28–35]. Wei et al. investigated a different compound MA_2KBiCl_6 with different starting materials by hydrothermal process [36]. However, no such reports are available, where, Group 1 elements like Sodium, Potassium were used to compensate the trivalent charge of bismuth occupied the mixed B-site along with lead in ABX_3 perovskite.

In the current investigation, we reduced 50% lead content by doping Group 1 (K/Na) and Group 15 (Bi) elements in these perovskites in order to attain better moisture stability. In single perovskite architecture replacement of Pb^{2+} with Bi^{3+} is difficult, since B site of ABX_3 perovskite has formal valence of (+2). Hence the simple substitution of Bi^{3+} in place of Pb^{2+} in $MAPbI_3$ was reported to result the formation of non-regular perovskite structure to maintain overall charge neutrality condition leading towards the increase in defect sites [37]. To troubleshoot all these issues, we explored triple cation B-site perovskites architecture by designing $A^{+}(B'^{+}_{0.25}B''^{3+}_{0.25})B'''^{2+}_{0.5}I_3$ structure, where $B' = Na$ or K, $B'' = Bi$ and $B''' = Pb$ based on tolerance factor (t) and octahedral factor (μ) calculation as shown in Fig. 1(a). Tolerance factor of MKBPI is similar to $MAPbI_3$. Whereas, the value of tolerance factor of MNBPI is closer to 1 compared to that of MKBPI. In general, perovskite compounds generate stable cubic structure, when $t \approx 1$ and $\mu \approx 0.6$ [38]. We synthesized $MAK_{0.25}Bi_{0.25}Pb_{0.5}I_3$ (MKBPI) and $MANa_{0.25}Bi_{0.25}Pb_{0.5}I_3$ (MNBPI) perovskite architecture (Fig. 1(b)) by solution processed crystallization method. To the best of our knowledge, it is the first report on synthesis and characterization of MKBPI and MNBPI perovskites.

Furthermore, we performed antisolvent treatment on the thin films of these perovskites as schematically shown in Fig. 2. Deposition of antisolvent drop on top of the wet perovskite film immediately after spin-coating promotes fast crystallization [39–42]. Ordered triangular and star shaped crystals were obtained for MKBPI and MNBPI, respectively due to antisolvent treatment. Both the perovskites exhibited very good thermal and moisture stability as evident by good optical absorption obtained in the UV–Vis spectroscopy even after keeping these thin-films at ambient atmosphere for 14 days.

2. Experimental section

2.1. Materials

Methyl amine (CH_3NH_2, aqueous, 40%, Acros Organic), Hydroiodic acid (HI, 57 wt% in H_2O, distilled, stabilized, 99.95%), Lead nitrate ($Pb(NO_3)_2$, 99%), Sodium iodide (NaI, ≥ 99.5%), Potassium iodide (KI, 99%) Bismuth iodide (BiI_3, 99.999%), Fluorine doped tin oxide (FTO) (~13Ω, TEC15) coated glasses (~13Ω, TEC15), anhydrous γ-butyrolactone (GBL), absolute ethanol, toluene (AR) and diethyl ether (Dry, AR), gold wire (99.99%), Titanium(IV) isopropoxide, (99.999%), 2,2′,7,7′-tetrakis(N,N-di-p-methoxyphenyl-amine)-9,99-spirobifluorene (spiro-MeOTAD, Merck), bis(trifluoromethane)sulfonimide lithium salt (Li-TFSI, 99.95%), 4-tert-butylpyridine (TBP, 96%), Titanium(IV) isopropoxide, (99.999%) were purchased from Sigma Aldrich. All the reagents except toluene were used without any further purification; Toluene was distilled before use.

2.2. Methylammonium iodide (MAI, CH_3NH_3I)

$$CH_3NH_2 + HI = CH_3NH_3I \quad (1)$$

MAI was synthesized by reacting HI (28 mL, dropwise) and CH_3NH_2 (18 mL) in a 150 mL round bottom flask (RBF) on an ice-water bath with continuous Argon purging and stirring. Temperature was carefully controlled between 0 and 5 °C. After 2 h, it was rotary evaporated. Yellowish product was dissolved in warm ethanol and kept for recrystallization. The product was washed with diethyl ether and dried overnight under vacuum at 60 °C.

2.3. Lead iodide (PbI_2)

$$Pb(NO_3)_2 + 2KI = PbI_2 + 2KNO_3 \quad (2)$$

Lead iodide was synthesized by reacting Lead nitrate and Potassium iodide in 1:2 M ratios in a 250 mL RBF (aqueous medium). Filtered product was dried in vacuum oven at 80 °C for 6 h.

2.4. Preparation of MKBPI and MNBPI thin films

$$4CH_3NH_3I + 2PbI_2 + BiI_3 + KI = 2(CH_3NH_3)_2(K_{0.5}Bi_{0.5})PbI_6 \quad (3)$$

$$4CH_3NH_3I + 2PbI_2 + BiI_3 + NaI = 2(CH_3NH_3)_2(Na_{0.5}Bi_{0.5})PbI_6 \quad (4)$$

Equivalent amount of CH_3NH_3I, KI, BiI_3 and PbI_2 were taken into a double necked RBF and dissolved in γ-butyrolactone (GBL) for MKBPI synthesis. The RBF was heated at 110 °C on silicone oil bath with constant stirring under argon atmosphere. Further dried under vacuum at 60 °C. Similar procedure was followed for MNBPI.

All the studied thin films were prepared on FTO coated glass substrates. The substrates were cleaned by sonication with soap (Hellmanex III) in deionized water (v/v = 2:100) followed by isopropanol and acetone/water mixture (v/v = 1:1). Before the deposition of perovskites, substrates were treated in a UV−O_3 chamber for 10 min.

For depositing perovskite layers, 0.88 M solution was prepared in GBL and kept overnight at 55 °C. The solution was spin coated on pre-heated FTO coated glass substrates at 3500 rpm for 30 s. Toluene drops were added just after 10 s of spin, followed by annealing at 100 °C for 10 min. Fig. 2 represented the schematic of thin film deposition process.

2.5. Preparation of solar cell devices

The FTO glass was used as a substrate for solar cell fabrication. For electron transport layer (ETL), TiO_2 sol was prepared using titanium tetra isopropoxide (TTIP) and ethanol (as solvent). A solution consisting of TTIP and ethanol was kept under the continuous vigorous stirring at

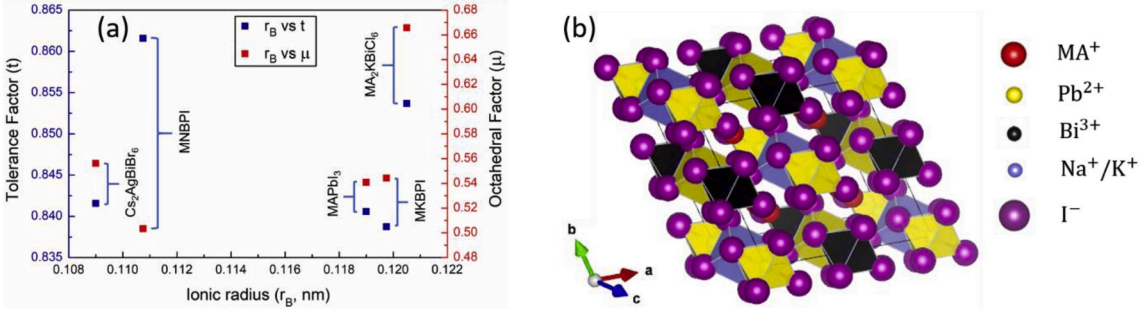

Fig. 1. Schematic representation of (a) tolerance and octahedral factor of different perovskites (b) MKBPI or MNBPI perovskite architecture with hexagonal symmetry.

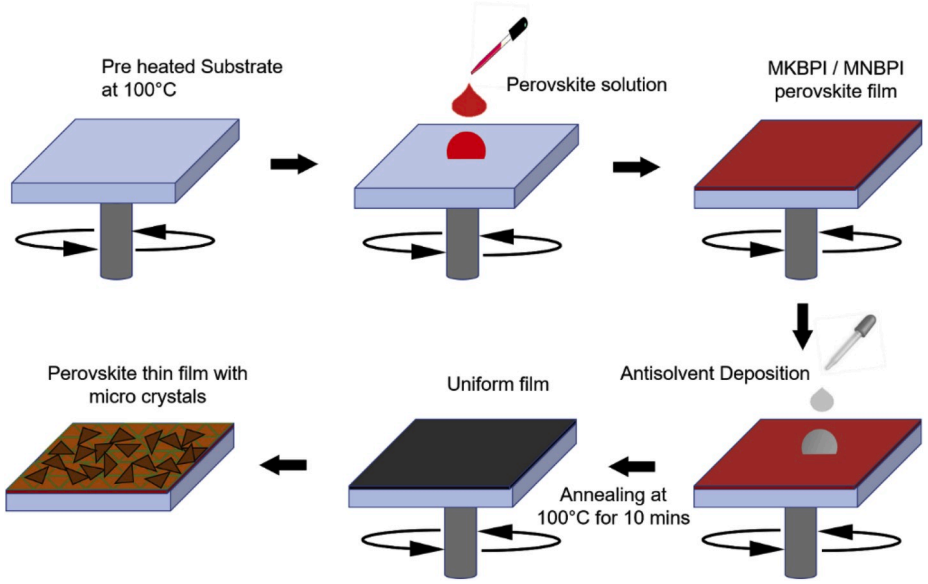

Fig. 2. Schematic representation of single step spin coating process with antisolvent treatment.

room temperature. After 30 min of continuous stirring transparent sol was obtained. The as-prepared TiO_2 sol was then spin coated on substrate at 4000 rpm for 30 s and subsequently sintered for 500 °C for 1 h with heating rate of 5 °C per minute to form a compact layer. Perovskite thin films (MKBPI and MNBPI) were then deposited by spin-coating. A hole-transporting layer (HTL) was deposited onto the perovskite film by spin coating at 3000 rpm for 30 s. The HTL solution contained 17.5 μL of bis(trifluoromethane)sulfonimide lithium salt solution (520 mg cm^{-3} Li-TFSI in 1 mL acetonitrile), 28.5 μL of 4-tert-butylpyridine (TBP), 72.3 mg of spiro-OMeTAD and 1 mL of chlorobenzene. We have finally used 50-nm thick gold as the counter electrode that was thermally evaporated on the top of the HTL.

2.6. Characterization

Fluorescence transients were recorded by using a commercial time correlated single photon counting (TCSPC) setup (LifeSpec-II, Edinburgh Instruments, UK). All samples were excited at 442 nm and the full width at half maxima of the instrument response function (IRF) is about 120 ps. The time-resolved fluorescences were fitted with sum of three exponentials along with the deconvolution with the IRF. UV–Vis spectroscopy was carried out in the visible region of sunlight using Cary 7000 model of Agilent Technologies' UV–Visible spectrophotometer. PerkinElmer "Spectrum Two" spectrometer was used to carry out FT-IR experiments from 1000 cm^{-1} to 3500 cm^{-1} of IR radiation. X-ray diffraction patterns were recorded by PANalytical X'Pert Powder diffractometer with Cu-Kα as incident radiation (λ = 0.154 nm) in the 2θ range between 5° and 60° with the step size of 0.020. Differential scanning calorimetry (DSC) and thermogravimetric analysis (TGA) was performed using a STA 8000 Perkin Elmer TGA/DSC system. All the Field emission scanning electron microscopy (FESEM) images of perovskite thin films were collected by NOVA NANOSEM 450 in secondary electron mode with accelerating voltage of 20 KV. Photoluminescence (PL) spectra of the perovskite active layer films were collected in Horiba Triax 320. The photocurrent voltage curves of the photovoltaic devices were performed using a Keithley 2420 source unit under simulated AM 1.5G spectrum at 100 mW/cm^2, irradiated by an Oriel 9600 solar simulator and the intensity was calibrated by Si reference cell.

3. Results and discussion

3.1. Morphological and structural study

In order to attain a comprehensive understanding of the effect of antisolvent on crystallization, the surface morphology of perovskite films was investigated by field emission scanning electron microscopy (FESEM). It is reported that the use of an antisolvent on top of the wet perovskite layer during spin coating induces fast crystallization, which assists large crystal formation as well as better surface coverage. In the present study, both MKBPI and MNBPI thin films were treated with chlorobenzene. Chlorobenzene was chosen as an anti-solvent since it did not dissolve the active perovskite constituents but miscible with GBL, which was chosen as solvent for spin coating the perovskite films. It is evident from Fig. 3(a) that compact, dense thin film was obtained from the chlorobenzene treated MKBPI. It is hypothesized that anti-solvent deposition over the perovskite films by spin coating followed by annealing at 100 °C, removed excess solvent swiftly, resulting super saturation promoted heterogeneous nucleation leading towards precipitation. Fig. 3(b) depicts dendritic crystal growth in MNBPI thin film surface. Star shaped large dendritic crystals (≈ 8.2 μm) were observed on the surface of the MNBPI film after the antisolvent treatment. It is to be noted here that MKBPI films, treated by chlorobenzene were almost pin-hole free with dense microstructure. The large size crystals obtained in these perovskite films can be helpful in reducing defects and trapped charges, leading towards enhanced intrinsic stability of the perovskites.

Furthermore, elemental color mappings of MKBPI and MNBPI compositions were carried out by the Energy Dispersive X-ray Spectroscopy to examine distributions of the constituents in thin films. Fig. 3(c) and (d) depicts that all the constituents (C, N, K/Na, Pb, Bi and I) are homogeneously distributed all over the thin films.

Room temperature XRD patterns of MKBPI and MNBPI thin films shown in Fig. 4 suggest the formation of single-phase solid solution of these halide perovskites as no such extra peaks corresponding to any secondary phase other than the FTO glass substrate, were found. The XRD profiles of both $MAK_{0.25}Bi_{0.25}Pb_{0.5}I_3$ and $MANa_{0.25}Bi_{0.25}Pb_{0.5}I_3$ were similar. Crystal structure of these perovskites determined by CELREF software was found to be hexagonal symmetry with $P6_3/mmc$ (194) space group as schematically shown in Fig. 1(b) for both materials. Lattice parameter of MKBPI was determined to be, a = b = 14.48 Å, c = 18.219 Å, whereas the lattice parameter of MNBPI was, found to be a = b = 14.344 Å, c = 18.926 Å. However, no difference was found in the

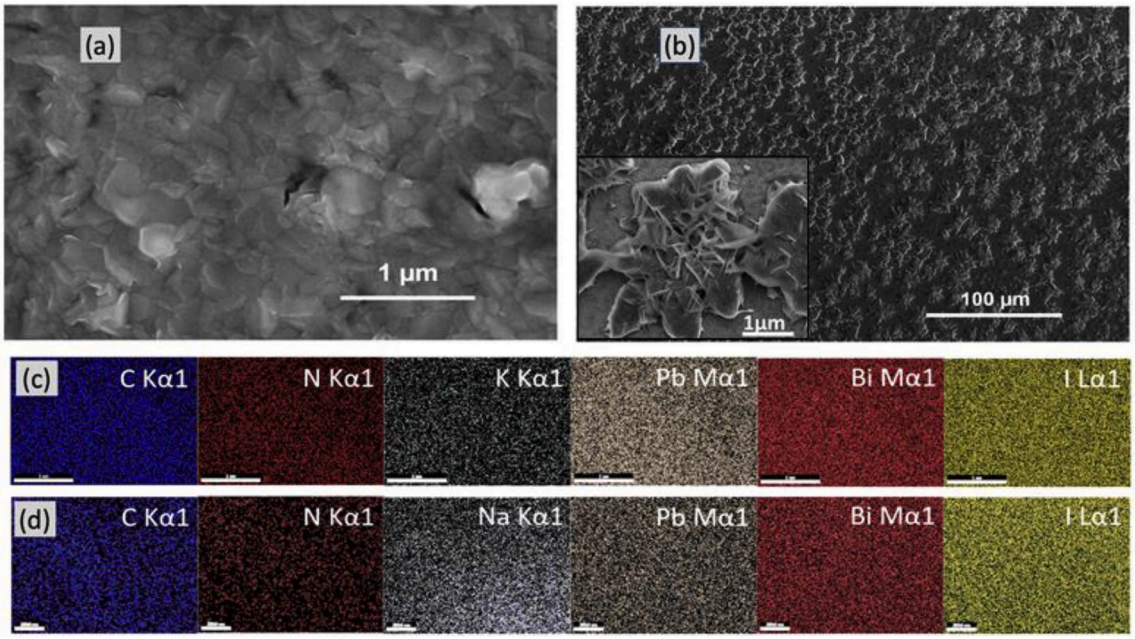

Fig. 3. FESEM images of (a) MKBPI and (b) MNBPI perovskite thin film after anti-solvent (chlorobenzene) treatment; Energy Dispersive X-ray Spectroscopy of (c) MKBPI and (c) MNBPI perovskite films showing elemental mappings.

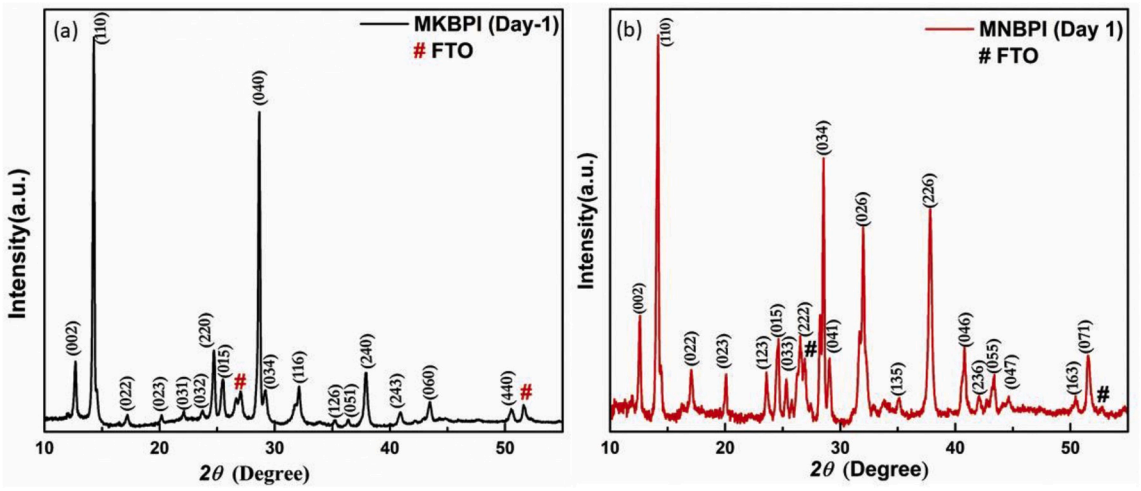

Fig. 4. Room temperature x-ray diffraction (XRD) profiles of (a) MKBPI and (b) MNBPI perovskite films.

XRD patterns of bulk and thin film of both materials. Our findings for MKBPI and MNBPI space groups are similar to the that of MBI reported in the literature [33,35].

3.2. Spectroscopic study

In order to know the functional groups and various bonds, we performed Fourier-transform infrared absorption (FTIR) of as-synthesized crystalline powder of MKBPI and MNBPI samples. Fig. 5 shows the FTIR transmittance spectrum of MKBPI and MNBPI recorded in the range of 1000–3150 cm^{-1}. The characteristic peaks occurred for N–H bending, C–H bending at 1466 cm^{-1}, 1575 cm^{-1} and 3116 cm^{-1}, respectively. Spectral absorption of the film is one of the key factors that effects the performance of thin film solar cells [43].

The UV–Visible spectral absorption of the MKBPI and MNBPI thin films were investigated at 400–800 nm. It can be observed from Fig. 6(a) that MKBPI sample exhibits decreasing trend in the absorption with increase in wavelength of light contrary to the MNBPI film which shows

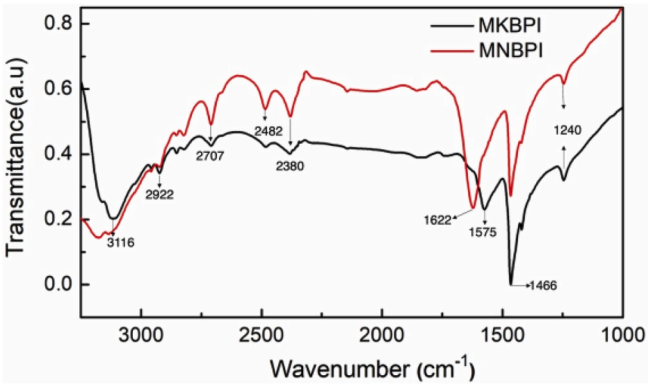

Fig. 5. FTIR transmittance spectra of (MKBPI) and (MNBPI).

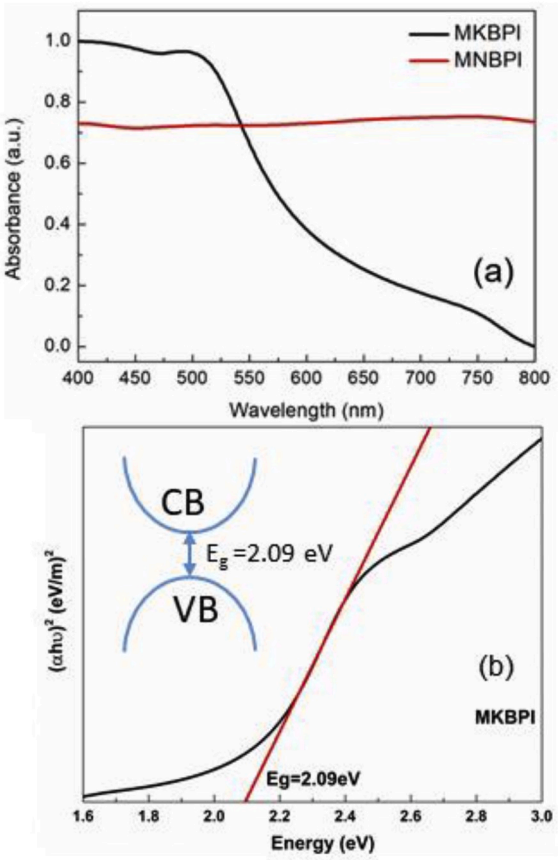

Fig. 6. UV–Vis spectra of as synthesized annealed thin film samples of (a) MKBPI and MNBPI (b) Tauc plot of MKBPI.

almost flat curve. A broad peak can be visualized in the graph for MKBPI sample, slope of which was used to determine its optical band gap (E_g) using Tauc formula, which is expressed by the following Equation (5) [44,45].

$$(\alpha h\nu)^k \propto (h\nu - E_g) \tag{5}$$

In the above equation, α represents absorption coefficient, and the value of k depicts the nature of the band gap. Perovskites, being direct band gap material, the value of k was taken as 2 [46]. The estimated optical direct band gap of MKPBI was found to be 2.09 eV as shown in Fig. 6(b). Interestingly, Bi-based similar hybrid perovskite materials showed higher bandgap compared to the current materials. Wei et al. reported methylammonium based perovskite MA_2KBiCl_6 with indirect bandgap of 3.04 Ev [36]. McClure et al. reported bandgap of 2.26 eV and 3.0 eV for cesium based perovskite materials such as $Cs_2AgBiBr_6$ and $Cs_2AgBiCl_6$ respectively [47,48]. In case of MNBPI film, we have not observed any sharp absorption peak, so it was difficult to estimate the band gap precisely from the Tauc plot.

To further elucidate the optical properties of the MKBPI and MNBPI, photoluminescence (PL) measurements were performed. It can be seen from the PL spectra shown in Fig. 7 that both MKBPI and MNBPI films demonstrated intense broad peak around 665 nm suggesting similar kind of electronic band gap for these two perovskites.

Time correlated single photon counting (TCSPC) technique was performed to understand the kinetics of photo-induced carriers, happening in its excited states. In this technique, molecules were excited by a very short pulse at t = 0, and decay of fluorescence in terms of photoluminescence counts was measured. 442 nm laser was used to excite the molecules, and the decays were probed at 530 nm. Fig. 8 depicts the fluorescence decays of both perovskites. This is the very first investigation on photo-induced fluorescence decay kinetics of triple cation based organic-inorganic hybrid perovskite. The MKBPI fluorescence decay was fitted to a bi-exponential decay model, and MNBPI fluorescence decay was fitted to a tri-exponential decay model to determine the relative concentrations of the extracted and the recombined charge-carriers and their respective charge-carrier lifetimes. We followed the following equations for determining the mean life time of decays.

$$I(t) = I(0)\sum_i A_i \exp\left(-t/\tau_i\right) \tag{6}$$

$$\tau_m = \frac{\int_i^\infty tI(t)\,dt}{\int_0^\infty I(t)\,dt} = \frac{\sum_i A_i\tau_i^2}{\sum_i A_i\tau_i} \tag{7}$$

Where, A_i and τ_i are the amplitude and lifetime of the different decay processes respectively.

The computed amplitude for each component was converted to express the percentage contribution of each component to the total fluorescence as:

$$A_i = \frac{A_i\tau_i}{\sum_i A_i\tau_i} * 100\% \tag{8}$$

As depicted in Table 1, 52% carriers in MKBPI experienced annihilation after 1 ns (ns), whereas 92% excitons in MNBPI, as shown in Table 2, had charge carrier lifetime of 36 ps (ps). Majority carriers in

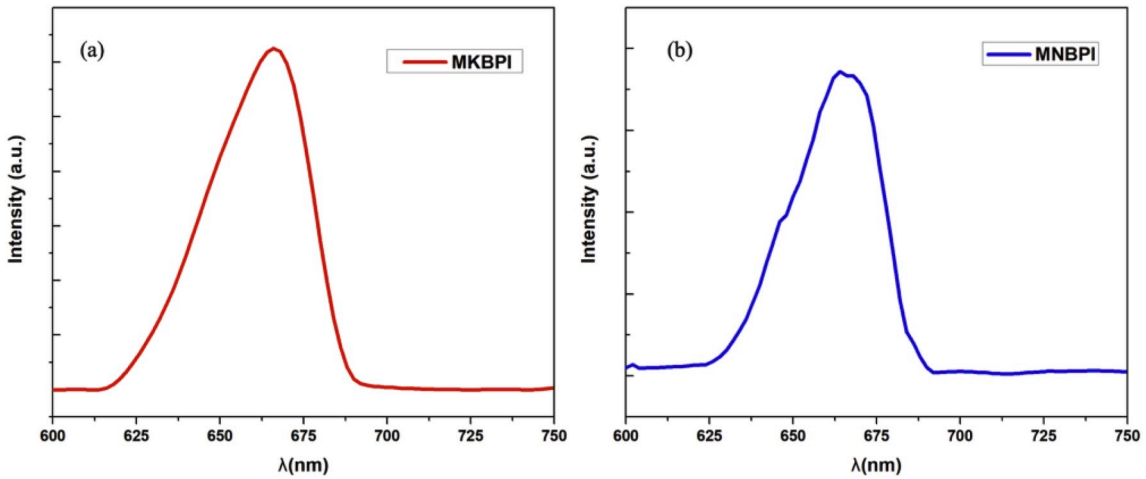

Fig. 7. Photoluminescence spectra of (a) MKBPI and (b) MNBPI at room temperature.

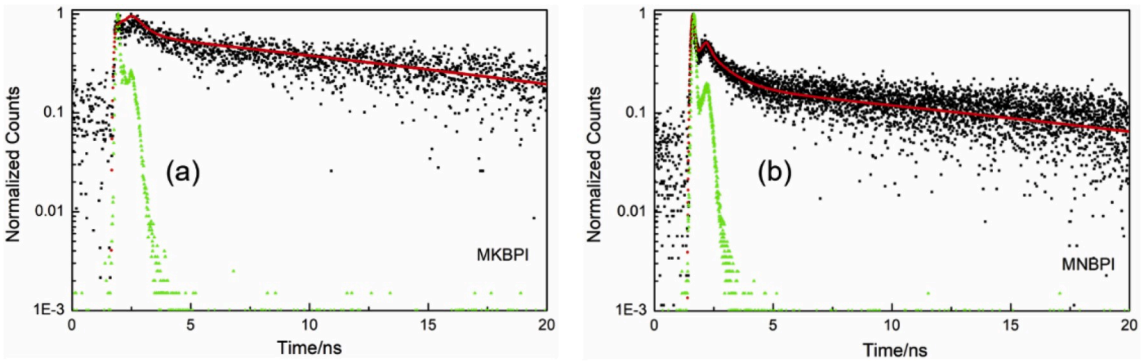

Fig. 8. Normalized TCSPC measurements for (a) MKBPI and (b) MNBPI perovskite layers on FTO coated glass.

Table 1
Bi-exponential decay model for MKBPI.

Composition	τ_1/ns	(A_1) %	τ_2/ns	(A_2) %	τ_m/ns
MKBPI	1.003	52	33.035	48	32.02

Table 2
Tri-exponential decay model for MNBPI.

Composition	τ_1/ps	(A_1) %	τ_2/ps	(A_2) %	τ_3/ns	(A_3) %	τ_m/ns
MNBPI	36	92	933	5	19.43	3	17.03

MKBPI experienced annihilation after 32.02 ns (ns), whereas excitons in MNBPI had charge carrier lifetime of 17.03 ns. It suggests that in our case, K incorporation in triple cations at B-site of perovskite exhibited a higher carrier lifetime than Na. Superior charge carrier lifetime of MKBPI can be attributed to the dense microstructure with better morphology, in which the triangular crystals obtained by equiaxed growth were connected to each other, unlike star-shaped MNBPI crystals formation due to dendritic crystal growth. In comparison, Ran et al. [26] demonstrated a carrier lifetime of 0.78 ns of MBI with better surface coverage in the thin film. Hoye et al. [24] achieved a charge carrier lifetime of 120 ps in solution-processed methylammonium bismuth iodide. Whereas their vapor assisted MBI exhibited a higher recombination time of 5.6 ns. Thus, we have increased, by order of magnitude, the charge-carrier-lifetime in MKBPI and MNBPI perovskites, as compared to any other Bi-based organometallic perovskites, as reported in the literature. It can be concluded that the triple cation at B-site with prevailing charge neutrality can be a good strategy to improve the charge carrier lifetime of in organometallic halide perovskites.

3.3. Thermal stability study

Thermal stability of MKBPI and MNBPI was investigated by thermogravimetric analysis (TGA) and differential scanning calorimetry (DSC) measurements in the temp range from room temperature to 830 °C. Change in slope of the temperature dependent weight loss curve derived from the TGA measurement suggest that the weight loss occurred at several steps from 293 °C to 743 °C in MKBPI and from 284 °C to 711 °C in MNBPI. All these weight losses corresponding to melting of methylammonium iodide, bismuth iodide and lead iodide are consistent with the DSC report of these compounds [49,50]. In DSC curve, both MKBPI and MNBPI perovskite exhibited a large exothermic peak at around 350 °C, similar to what was reported earlier for the melting of MAI [49]. Most importantly DSC curve implies no signature of any exothermic or endothermic reaction below 280 °C. Also, the slope of the TGA curve was found to be constant below 280 °C as evident from the flat curve of TGA shown in Fig. 9. DSC and TGA results validate the thermal stability of these perovskite materials up to 280 °C.

3.4. Degradation study

Furthermore, we carried out degradation studies of the perovskite films kept in ambient air by measuring their UV–visible absorption spectrum and XRD. During two weeks of exposure to ambient atmosphere in India, the temperature varied from 30 °C to 42 °C and relative humidity changed from 40% to 80% respectively. Moreover, these thin film samples were not coated with any metal or passivation layer on top of it, giving complete exposure of the perovskite layer to the atmosphere. It was observed in XRD that MNBPI and MKBPI compounds were not degraded in 7 days as shown in Fig. 10. However, few extra peaks corresponding with PbI_2 observed in the X-ray diffraction patterns after 14 days suggesting the beginning of degradation of sample. It was to be noted that $MAPbI_3$ perovskites degrades much faster, actually in few minutes to hours' time. It suggests that current samples are lot more

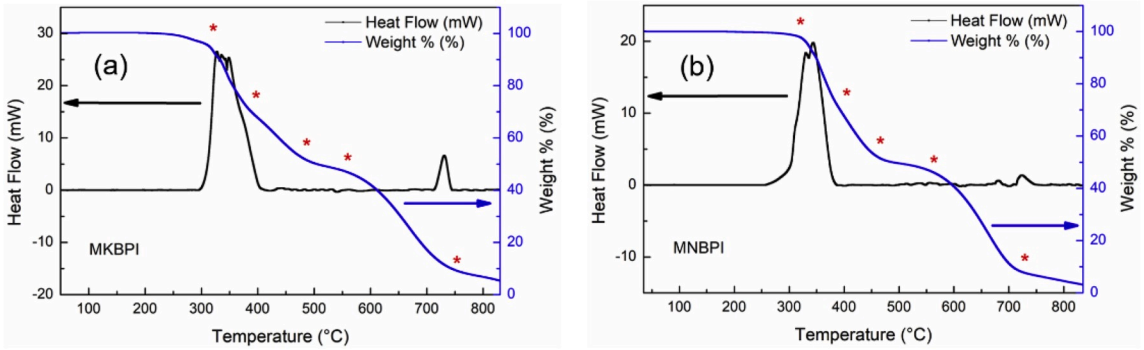

Fig. 9. Thermogravimetric heating curve and differential scanning calorimetry curve of (a) MKBPI and (b) MNBPI.

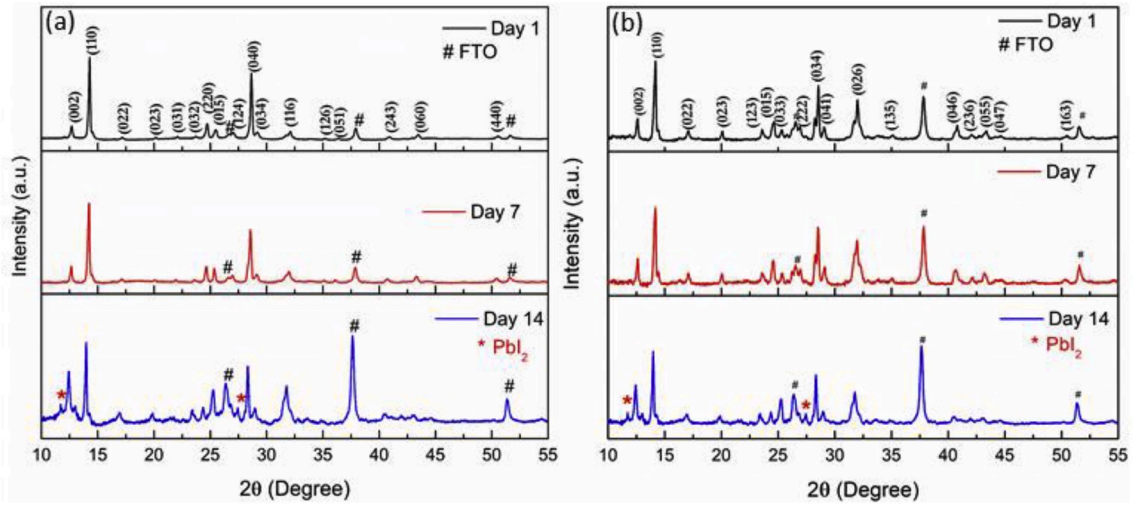

Fig. 10. X-ray diffraction (XRD) patterns of (a) MKBPI and (b) MNBPI perovskite films.

stable than $MAPbI_3$.

The UV–visible spectroscopy was also performed at different time intervals to check the stability of the perovskite films as shown in Fig. 11. Both these perovskites exhibited strong optical absorption even after two weeks implying much better stability than that of $MAPbI_3$ perovskite [12], which further validates our XRD results. Since these thin-film samples were kept bare to the open atmosphere, it is anticipated that the use of an HTM layer and a layer of metal electrode in practical solar cell architecture will prevent these films from direct exposure to moisture and heat. So, it is expected that these perovskites will provide significant operational time, which is the requirement of commercialization of these solar cell materials.

3.5. Solar cell device performance

Fig. 12 shows the J-V curve of as-fabricated solar cells using MKBPI and MNBPI. MKBPI and MNBPI based perovskite solar cells demonstrated the efficiency of 0.14% and 0.031%, respectively. It can be seen from Table 3 that the fill factors of these cells are as low as 27% and 38% for MNBPI and MKBPI respectively, which is one of the main factors for the less performance of the bismuth-based perovskite solar cell. It is to be noted that Senol et al. and Chunfeng et al. also reported the solar cell efficiency of 0.1% and 0.076% respectively [51,52]. By using Vacuum vapor deposition of $MA_3Bi_2I_9$ perovskite active layer, Jiachi et al. have also tried to improve the morphology of the perovskite active layers and reported the efficiency of 0.063% [53]. In our present work, the less compact structure of MNBPI as compared to MKBPI based active layer film might be the reason of less solar cell efficiency. Also, the further optimization is needed in selection, processing and thickness monitoring

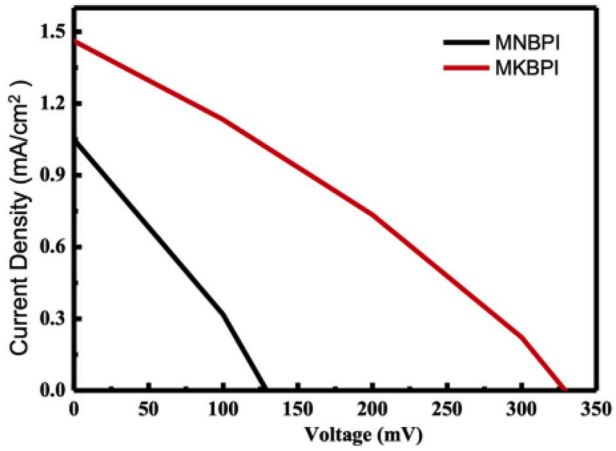

Fig. 12. J–V curves Of MKBPI and MNBPI based solar cells.

Table 3
Photovoltaic performance of MNBPI & MKBPI perovskite materials Material.

Materials	Voc (mV)	Jsc (mA/cm^2)	Fill factor	Efficiency (%)
MNBPI	128.8	1.04	0.27	0.031
MKBPI	327.6	1.46	0.38	0.14

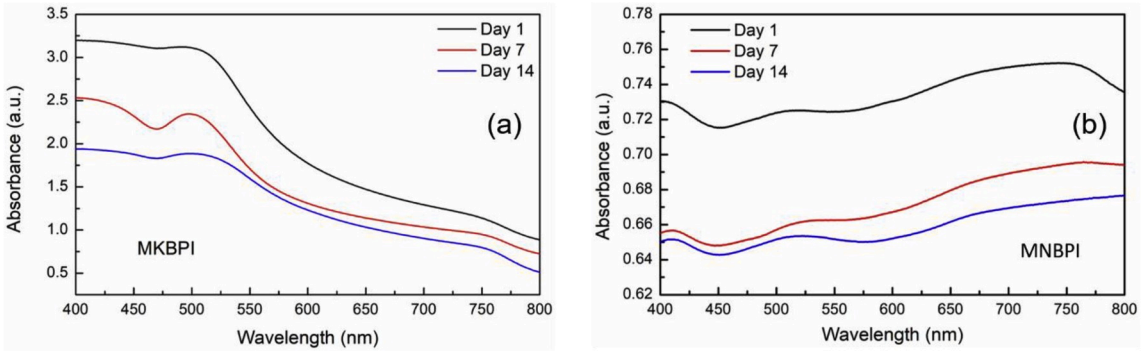

Fig. 11. UV–visible absorption spectra of (a) MKBPI and (b) MNBPI active layer thin film.

of ETM and HTM to increase the efficiency of these devices. Nevertheless, its advantages of less toxicity and ambient stability are still promising for the fabrication of perovskite solar cell devices.

4. Conclusion

In summary, we synthesized partially lead free organic-inorganic hybrid perovskite photo absorber materials viz. $MAK_{0.25}Bi_{0.25}Pb_{0.5}I_3$ and $MANa_{0.25}Bi_{0.25}Pb_{0.5}I_3$ with low band gap, for application in perovskite solar cell. We showed that replacing 50% lead content in the B site of ABX_3 perovskite by bismuth and potassium or sodium, superior moisture resistant, stable perovskite could be made. These new compounds crystallized in hexagonal structure with $P6_3/mmc$ space group. Both the perovskite thin films demonstrated good absorption coefficient in the visible spectrum. Moreover, these materials showed order of magnitude higher charge carrier lifetime compared to Bi-based halide perovskites previously reported in the literature. We also found that both materials were thermally stable up to 280 °C with no detectable signature of exothermic or endothermic reaction correspond to materials decomposition determined from the TGA and DSC measurement. Moreover, our synthesized perovskites showed remarkable stability in the hot and humid climate. Current work on MKBPI and MNBPI compounds suggests that using multiple cations in B-site with satisfying charge neutrality condition can be potential way of engineering stable lead-free organometallic halide photovoltaic materials for the future design of solar cell devices.

Novelty statement

In this work, we have synthesized two novel, organometallic halide-based tetra-cation perovskite photo-absorbers $CH_3NH_3K_{1/4}Bi_{1/4}Pb_{1/4}I_3$ (MKBPI) and $CH_3NH_3Na_{1/4}Bi_{1/4}Pb_{1/4}I_3$ (MNBPI) for solar cell applications. We reduced 50% lead content by incorporating Group 1 (Na/K) and Group 15 (Bi) elements in perovskite lattices in order to attain better moisture stability without compromising energy conversion capability by designing triple cations B-site perovskite architecture.

To the best of our knowledge, this is the first report on synthesis and characterization of MKBPI and MNBPI perovskites. We studied their optical absorption, fluorescence decay kinetics and thermal stability. Moreover, we studied their degradation behavior. Both of these new compounds exhibited very good optical absorption in the UV–Vis spectroscopy even after keeping the samples at ambient atmosphere for 14 days without any top layer.

Currently, almost all the efficient organometallic halides-based perovskite solar cells are lead based i.e. methylammonium lead iodide ($CH_3NH_3PbI_3$). However, considering the toxic and environmentally hazardous nature of lead, it is of paramount concern to develop stable lead-free PSC. We believe that our new findings present a recipe of designing novel lead-free, stable tetra-cation perovskite solar cell materials.

Declaration of competing interest

The authors declare that they have no known competing financial interests or personal relationships that could have appeared to influence the work reported in this paper.

CRediT authorship contribution statement

Pritam Dey: Methodology, Formal analysis, Writing - original draft, Writing - review & editing. **Harish Singh:** Methodology, Formal analysis, Writing - review & editing. **Rahul K. Gupta:** Methodology, Formal analysis. **Debabrata Goswami:** Formal analysis, Writing - review & editing. **Tanmoy Maiti:** Conceptualization, Formal analysis, Writing - review & editing, Supervision.

References

[1] M.A. Green, A. Ho-Baillie, Perovskite solar cells: the birth of a new era in photovoltaics, ACS Energy Lett. 2 (2017) 822–830.

[2] D. Weber, $CH_3NH_3SnBrxl_3$ x (x = 0-3), ein Sn(II)-System mit kubischer Perowskitstruktur CHsNHsSnBraJa-z = 0-3), a Sn(II)-System with Cubic Perovskite Structure, 1978.

[3] D. Weber, $CH_3NH_3PbX_3$, ein Pb (II)-System mit kubischer Perowskitstruktur/ $CH_3NH_3PbX_3$, a Pb (II)-System with Cubic Perovskite Structure, Z. Naturforsch. B Chem. Sci. 33 (1978) 1443–1445.

[4] A. Kojima, K. Teshima, Y. Shirai, T. Miyasaka, Organometal halide perovskites as visible-light sensitizers for photovoltaic cells, J. Am. Chem. Soc. 131 (2009) 6050–6051.

[5] W.S. Yang, B.W. Park, E.H. Jung, N.J. Jeon, Y.C. Kim, D.U. Lee, S.S. Shin, J. Seo, E. K. Kim, J.H. Noh, S. Il Seok, Iodide management in formamidinium-lead-halide-based perovskite layers for efficient solar cells, Science 356 (2017) 1376–1379.

[6] G. Xing, N. Mathews, S. Sun, S.S. Lim, Y.M. Lam, M. Graẗzel, S. Mhaisalkar, T. C. Sum, Long-range balanced electron-and hole-transport lengths in organic-inorganic CH3NH3PbI3, Science 342 (2013) 344–347.

[7] S.D. Stranks, G.E. Eperon, G. Grancini, C. Menelaou, M.J.P. Alcocer, T. Leijtens, L. M. Herz, A. Petrozza, H.J. Snaith, Electron-hole diffusion lengths exceeding 1 micrometer in an organometal trihalide perovskite absorber, Science 342 (2013) 341–344.

[8] G.E. Eperon, V.M. Burlakov, P. Docampo, A. Goriely, H.J. Snaith, Morphological control for high performance, solution-processed planar heterojunction perovskite solar cells, Adv. Funct. Mater. 24 (2014) 151–157.

[9] N.-K. Kim, Y.H. Min, S. Noh, E. Cho, G. Jeong, M. Joo, S.-W. Ahn, J.S. Lee, S. Kim, K. Ihm, Investigation of thermally induced degradation in $CH_3NH_3PbI_3$ perovskite solar cells using in-situ synchrotron radiation analysis, Sci. Rep. 7 (2017) 4645.

[10] L. Zhang, M. Ju, WanZhen Liang, The effect of moisture on the structures and properties of lead halide perovskites: a first-principles theoretical investigation, Phys. Chem. Chem. Phys. 18 (2016) 23174–23183, undefined.

[11] S.N. Habisreutinger, T. Leijtens, G.E. Eperon, S.D. Stranks, R.J. Nicholas, H. J. Snaith, Carbon nanotube/polymer composites as a highly stable hole collection layer in perovskite solar cells, Nano Lett. 14 (2014) 5561–5568.

[12] G. Flora, D. Gupta, A. Tiwari, Toxicity of lead: a review with recent updates, Interdiscipl. Toxicol. 5 (2012) 47–58.

[13] A.A. Ab Latif Wani, J.A. Usmani, Lead toxicity: a review, Interdiscipl. Toxicol. 8 (2015) 55.

[14] I.C. Smith, E.T. Hoke, D. Solis-Ibarra, M.D. McGehee, H.I. Karunadasa, A layered hybrid perovskite solar-cell absorber with enhanced moisture stability, Angew. Chem. Int. Ed. 53 (2014) 11232–11235.

[15] C.M.M. Soe, W. Nie, C.C. Stoumpos, H. Tsai, J.C. Blancon, F. Liu, J. Even, T. J. Marks, A.D. Mohite, M.G. Kanatzidis, Understanding film formation morphology and orientation in high member 2D Ruddlesden–Popper perovskites for high-efficiency solar cells, Adv. Energy Mater 8 (2018) 1700979.

[16] J. Qiu, Y. Xia, Y. Zheng, W. Hui, H. Gu, W. Yuan, H. Yu, L. Chao, T. Niu, Y. Yang, X. Gao, Y. Chen, W. Huang, 2D intermediate suppression for efficient ruddlesden-Popper (RP) phase lead-free perovskite solar cells, ACS Energy Lett. 4 (2019) 1513–1520.

[17] F. Giustino, H.J. Snaith, Toward lead-free perovskite solar cells, ACS Energy Lett. 1 (2016) 1233–1240.

[18] A. Ganose, C. Savory, David O. Scanlon, Beyond methylammonium lead iodide: prospects for the emergent field of ns 2 containing solar absorbers, Chem. Commun. 53 (2017) 20–44, undefined.

[19] Y. Li, W. Sun, W. Yan, S. Ye, H. Rao, H. Peng, Z. Zhao, Z. Bian, Z. Liu, H. Zhou, C. Huang, 50% Sn-based planar perovskite solar cell with power conversion efficiency up to 13.6%, Adv. Energy Mater. 6 (2016).

[20] F. Zuo, S.T. Williams, P.W. Liang, C.C. Chueh, C.Y. Liao, A.K.Y. Jen, Binary-metal perovskites toward high-performance planar-heterojunction hybrid solar cells, Adv. Mater. 26 (2014) 6454–6460.

[21] F. Hao, C.C. Stoumpos, D. Cao, R.P.H Chang, M.G Kanatzidis, et al., Lead-free solid-state organic–inorganic halide perovskite solar cells, Nat. Photonics 8 (2014) 489–494, https://doi.org/10.1038/nphoton.2014.82. In this issue.

[22] N. Noel, S. Stranks, Antonio Abate, Lead-free organic–inorganic tin halide perovskites for photovoltaic applications, Energy Environ. Sci. 7 (2014) 3061–3068, undefined.

[23] C.C. Stoumpos, C.D. Malliakas, M.G. Kanatzidis, Semiconducting tin and lead iodide perovskites with organic cations: phase transitions, high mobilities, and near-infrared photoluminescent properties, Inorg. Chem. 52 (2013) 9019–9038.

[24] R.L.Z. Hoye, R.E. Brandt, A. Osherov, V. Stevanovic, S.D. Stranks, M.W.B. Wilson, H. Kim, A.J. Akey, J.D. Perkins, R.C. Kurchin, J.R. Poindexter, E.N. Wang, M. G. Bawendi, V. Bulovic, T. Buonassisi, Methylammonium bismuth iodide as a lead-free, stable hybrid organic-inorganic solar absorber, Chem. Eur J. 22 (2016) 2605–2610.

[25] Y. Lyu, J.-H. Cai, Yalong, Paul Bernhardt, W. Zhang, H. Wang, Liu Gang, Wang, Organic–inorganic bismuth (III)-based material: a lead-free, air-stable and solution-processable light-absorber beyond organolead perovskites, Springer 9 (2016) 692–702.

[26] C. Ran, Z. Wu, J. Xi, F. Yuan, H. Dong, T. Lei, X. He, X. Hou, Construction of compact methylammonium bismuth iodide film promoting lead-free inverted planar heterojunction organohalide solar cells with open-circuit voltage over 0.8 V, J. Phys. Chem. Lett. 8 (2017) 394–400.

[27] P. Dey, V. Khorwal, P. Sen, K. Biswas, T. Maiti, Spectral studies of lead-free organic-inorganic hybrid solid-state perovskites $CH_3NH_3Bi_{2/3}I_3$ and CH3NH3Pb1/2Bi1/3I3: potential photo absorbers, ChemistrySelect 3 (2018) 794–800.

[28] M. Pazoki, M.B. Johansson, H. Zhu, P. Broqvist, T. Edvinsson, G. Boschloo, E.M. J. Johansson, Bismuth iodide perovskite materials for solar cell applications: electronic structure, optical transitions, and directional charge transport, J. Phys. Chem. C 120 (2016) 29039–29046.
[29] S. Sun, S. Tominaka, J.H. Lee, F. Xie, P.D. Bristowe, A.K. Cheetham, Synthesis, crystal structure, and properties of a perovskite-related bismuth phase, $(NH_4)_3Bi_2I_9$, Apl. Mater. 4 (2016).
[30] M. Vigneshwaran, T. Ohta, S. Iikubo, G. Kapil, T.S. Ripolles, Y. Ogomi, T. Ma, S. S. Pandey, Q. Shen, T. Toyoda, K. Yoshino, T. Minemoto, S. Hayase, Facile synthesis and characterization of sulfur doped low bandgap bismuth based perovskites by soluble precursor route, Chem. Mater. 28 (2016) 6436–6440.
[31] H. Wang, J. Tian, K. Jiang, Y. Zhang, H. Fan, J. Huang, L.-m. Yang, B. Guan, Y. Song, Fabrication of methylammonium bismuth iodide through interdiffusion of solution-processed BiI $_3$/CH_3NH_3I stacking layers, RSC Adv. 7 (2017) 43826–43830.
[32] B.W. Park, B. Philippe, X. Zhang, H. Rensmo, G. Boschloo, E.M.J. Johansson, Bismuth based hybrid perovskites A3Bi2I9 (A: methylammonium or cesium) for solar cell application, Adv. Mater. 27 (2015) 6806–6813.
[33] A.J. Lehner, D.H. Fabini, H.A. Evans, C.A. Hébert, S.R. Smock, J. Hu, H. Wang, J. W. Zwanziger, M.L. Chabinyc, R. Seshadri, Crystal and electronic structures of complex bismuth iodides $A_3Bi_2I_9$ (A = K, Rb, Cs) related to perovskite: aiding the rational design of photovoltaics, Chem. Mater. 27 (2015) 7137–7148.
[34] R. Jakubas, L. Sobczyk, Phase transitions in alkylammonium halogenoantimonates and bismuthates, Phase Transitions 20 (1990) 163–193.
[35] R. Jakubas, J. Zaleski, L. Sobczyk, Phase transitions in (CH3NH3)3Bi2I9 (MAIB), Ferroelectrics 108 (1990) 109–114.
[36] F. Wei, Z. Deng, S. Sun, F. Xie, G. Kieslich, D.M. Evans, M.A. Carpenter, P. D. Bristowe, A.K. Cheetham, The synthesis, structure and electronic properties of a lead-free hybrid inorganic–organic double perovskite $(MA)_2KBiCl_6$ (MA= methylammonium), Mater. Horizons 3 (2016) 328–332.
[37] K. Eckhardt, V. Bon, J. Getzschmann, J. Grothe, F.M. Wisser, S. Kaskel, Crystallographic insights into $(CH_3NH_3)_3(Bi_2I_9)$: a new lead-free hybrid organic–inorganic material as a potential absorber for photovoltaics, Chem. Commun. 52 (2016) 3058–3060.
[38] M.A. Green, A. Ho-Baillie, H.J. Snaith, The emergence of perovskite solar cells, Nat. Photon. 8 (2014) 506–514.
[39] M. Xiao, F. Huang, W. Huang, Y. Dkhissi, Y. Zhu, J. Etheridge, A. Gray-Weale, U. Bach, Y.B. Cheng, L. Spiccia, A fast deposition-crystallization procedure for highly efficient lead iodide perovskite thin-film solar cells, Angew. Chem. Int. Ed. 53 (2014) 9898–9903.
[40] N.J. Jeon, J.H. Noh, Y.C. Kim, W.S. Yang, S. Ryu, S. Il Seok, Solvent engineering for high-performance inorganic-organic hybrid perovskite solar cells, Nat. Mater. 13 (2014) 897–903.
[41] J.H. Heo, S.H. Im, J.H. Noh, T.N. Mandal, C.-S. Lim, J.A. Chang, Y.H. Lee, H.-j. Kim, A. Sarkar, M.K. Nazeeruddin, Efficient inorganic-organic hybrid heterojunction solar cells containing perovskite compound and polymeric hole conductors, Nat. Photon. 7 (2013) 486–491.
[42] W. Nie, H. Tsai, R. Asadpour, J.-C. Blancon, A.J. Neukirch, G. Gupta, J.J. Crochet, M. Chhowalla, S. Tretiak, M.A. Alam, High-efficiency solution-processed perovskite solar cells with millimeter-scale grains, Science 347 (2015) 522–525.
[43] N.-G. Park, Perovskite solar cells: an emerging photovoltaic technology, Mater. Today 18 (2015) 65–72.
[44] J. Tauc, Optical properties and electronic structure of amorphous Ge and Si, Mater. Res. Bull. 3 (1968) 37–46.
[45] R. Bhatt, I. Bhaumik, S. Ganesamoorthy, A.K. Karnal, M.K. Swami, H.S. Patel, P. K. Gupta, Urbach tail and bandgap analysis in near stoichiometric LiNbO 3 crystals, Phys. Status Solidi Appl. Mater. Sci. 209 (2012) 176–180.
[46] H.-S. Kim, C.-R. Lee, J.-H. Im, K.-B. Lee, T. Moehl, A. Marchioro, S.-J. Moon, R. Humphry-Baker, J.-H. Yum, J.E. Moser, M. Grätzel, N.-G. Park, Lead iodide perovskite sensitized all-solid-state submicron thin film mesoscopic solar cell with efficiency exceeding 9%, Sci. Rep. 2 (2012) 591.
[47] E.T. McClure, M.R. Ball, W. Windl, P.M. Woodward, Cs2AgBiX6 (X = Br, Cl): new visible light absorbing, lead-free halide perovskite semiconductors, Chem. Mater. 28 (2016) 1348–1354.
[48] A.H. Slavney, T. Hu, A.M. Lindenberg, H.I. Karunadasa, A bismuth-halide double perovskite with long carrier recombination lifetime for photovoltaic applications, J. Am. Chem. Soc. 138 (2016) 2138–2141.
[49] A. Dualeh, P. Gao, S. Il Seok, M.K. Nazeeruddin, M. Grätzel, Thermal behavior of methylammonium lead-trihalide perovskite photovoltaic light harvesters, Chem. Mater. 26 (2014) 6160–6164.
[50] A. Cuña, I. Aguiar, A. Gancharov, M. Pérez, L. Fornaro, Correlation between growth orientation and growth temperature for bismuth tri-iodide films, Cryst. Res. Technol. 39 (2004) 899–905.
[51] S. Öz, J.C. Hebig, E. Jung, T. Singh, A. Lepcha, S. Olthof, F. Jan, Y. Gao, R. German, P.H.M. van Loosdrecht, K. Meerholz, T. Kirchartz, S. Mathur, Zero-dimensional $(CH_3NH_3)_3Bi_2I_9$ perovskite for optoelectronic applications, Sol. Energy Mater. Sol. Cells 158 (2016) 195–201.
[52] C. Lan, J. Luo, S. Zhao, C. Zhang, W. Liu, S. Hayase, T. Ma, Effect of lead-free $(CH_3NH_3)_3Bi_2I_9$perovskite addition on spectrum absorption and enhanced photovoltaic performance of bismuth triiodide solar cells, J. Alloys Compd. 701 (2017) 834–840.
[53] J. Huang, Z. Gu, X. Zhang, G. Wu, H. Chen, Lead-free $(CH_3NH_3)_3Bi_2I_9$ perovskite solar cells with fluorinated PDI films as organic electron transport layer, J. Alloys Compd. 767 (2018) 870–876.